Computer Assisted Mechanics and Engineering Sciences, 14: 79–89, 2007.

Interaction of surface and internal cracks in railhead

Manicka Dhanasekar, Jian-Jun Han
Centre for Railway Engineering, Central Queensland University
Rockhampton, QLD 4702, Australia

Qing Hua Qin
Department of Engineering, Australian National University
Canberra, ACT 0200, Australia

(Received April 1, 2005)

This paper presents a two-dimensional model for the analysis of interaction between surface and internal cracks in the railheads subjected to wheel loading. The shape of the railhead, the surface crack and the internal crack are modelled as curved cracks defined by the theory of continuous distribution of dislocation in an infinite body. From the boundary conditions along these cracks, a system of singular integral equations is deduced. Influence functions in these singular integral equations are first expanded into the Cauchy kernel multiplying normal functions and later are reduced to a system of linear equations and solved numerically. Stress intensity factors (SIFs) of the surface crack tip are calculated from the numerical solution of distribution function along these cracks directly, eliminating need for any indirect integral method. The method does not require meshing and hence idealisation of the shapes of the cracks, thereby improving accuracy and reducing pre- and post processing efforts. Interaction between the internal crack and the surface crack is examined in detail through several examples.

Keywords: railhead, surface crack, internal crack, curved crack, SIF, crack angle

1. Introduction

Railheads are subjected to wheel/rail rolling contact fatigue loading that generates surface defects such as squats, shelling, and head checks, as well as internal material defects such as tache ovales, vertical split heads, surface cracks, etc. These defects significantly reduce safety and reliability of the rail transport operation because fully developed surface and/ or internal cracks can ultimately lead to complete failure of the rail. Furthermore, these defects adversely affect the riding comfort and the rolling noise. Currently the rail industry removes the surface cracks through rail grinding and "manages" the internal crack growth by minimising the wheel/rail contact loading, both at very high cost. Where surface cracks are accompanied by internal cracks, their interaction is not well understood. The objective of the paper is, therefore, to examine the interaction between these two categories of cracks under various wheel/rail contact loading regimes.

Crack interaction is firstly investigated for solving microcrack shielding problems. Interaction between two cracks in homogeneous bodies using a "pseudo-traction" method was examined in [6, 9, 10]. The authors of these papers have modelled the interaction problem by superposition of several sub problems in which one single crack in an infinite plane has been loaded by pseudo-traction along its crack faces. Employing the Green's functions of a single crack subjected to concentrated forces on the crack faces, the interaction problem is reduced into integral equations from the traction-free conditions along all the crack faces. From the numerical solutions to the integral equations, pseudo-traction along all the crack faces is evaluated. Using this method, the interaction problems for piezoelectric materials in particular the interaction between the interface and sub-interface cracks have been investigated in [3, 4, 12].

Following the pioneering work by Bilby *et al.* [1, 2] on the modelling of a single crack using continuously distributed dislocations, the dislocation method has been extended to treat the interaction between cracks and circular inclusions in [5]. For representing arbitrarily shaped internal cracks in finite size solids, the first two authors of this paper [8] developed a 2D dislocation modelling method. Long cracks embedded in finite solids were modelled with this method; practical issues such as the crack closure, or crack surface pressure have not been explored; surface crack modelling was also not addressed. This paper extends the method for examining the interaction between surface and internal cracks in finite solids; for this purpose the method was first modified to account for surface cracks. The method considers the problem as the superposition of two "curved cracks" residing in an infinite two dimensional continuum. All cracks have been modelled as continuous distribution of dislocation. From the boundary condition along these cracks, a system of singular integral equations has been deduced. To solve the singular integral equations for arbitrarily shaped cracks, influence functions in the integrals have been expanded into products of the Cauchy kernel with normal functions. Then the singular integral equations are further reduced to a system of linear equations and are solved numerically. Stress intensity factors of the surface crack tip are calculated from the numerical solution of the distribution function along these cracks. Interaction between the surface and internal cracks are finally discussed through several problems of railheads containing cracks.

The model presented in this paper could best be described as an alternate method to the finite element method widely used for solving crack problems. The advantage is that the method does not require meshing, thereby avoiding idealisation of the shape of the cracks, which may adversely affect the results. In spite of this, the method still uses numerical solution technique; therefore, could not be regarded as an analytical method.

2. FORMULATION

The stress (σ_{xx} , σ_{yy} , τ_{xy}) and displacement (u_x , u_y) in two dimensional elastic bodies are defined in terms of Muskhelishvili complex stress functions $\phi(z)$ and $\psi(z)$ [1] as shown in Eqs. (1) and (2), respectively,

$$\begin{aligned} \sigma_{xx} + \sigma_{yy} &= 2\left[\Phi(z) + \overline{\Phi(z)}\right], \\ \sigma_{yy} - \sigma_{xx} + 2\mathrm{i}\tau_{xy} &= 2\left[\overline{z}\Phi'(z) + \Psi(z)\right], \end{aligned} \tag{1}$$

$$2G(u_x + \mathrm{i}u_y) = \kappa\phi(z) - z\overline{\Phi(z)} - \psi(z), \tag{2}$$

where the over bar represents the conjugate of the complex function; and $\Phi(z) = \phi'(z)$, $\Psi(z) = \psi'(z)$, and $\kappa = (3-\nu)/(1+\nu)$ for plane stress, $\kappa = 3-4\nu$ for plane strain, in which ν and G are Poisson's ratio and the shear modulus of the material respectively.

A solution to an edge dislocation at pointz_a in an infinite plane was presented in [2],

$$\begin{aligned} \Phi(z) &= \frac{A}{(z-z_a)}, \\ \Psi(z) &= \frac{\overline{A}}{(z-z_a)} + \frac{A\overline{z_a}}{(z-z_a)^2}, \end{aligned} \tag{3}$$

where

$$A = \frac{G(\beta_x + \mathrm{i}\beta_y)}{[\mathrm{i}\pi(1+\kappa)]} \tag{4}$$

in which β_x and β_y are the Burgers vectors that represent the displacement due to the movement of dislocation.

The normal and the tangential stress components at a point z induced from the dislocation at z_a are derived by substituting Eq. (3) into Eq. (1) and employing (t, n) coordinates with incline angle θ,

$$\sigma_{nn} + \mathrm{i}\tau_{nt} = \beta_x f_x(z, z_a) + \beta_y f_y(z, z_a) \tag{5}$$

where

$$\begin{aligned} f_x(z, z_a) &= \frac{G}{\pi \mathrm{i}(1+\kappa)} \left(\frac{1}{z - z_a} - \frac{1}{\overline{z} - \overline{z_a}} - e^{2\mathrm{i}\theta} \left[\frac{1}{z - z_a} + \frac{(\overline{z} - \overline{z_a})}{(z - z_a)^2} \right] \right), \\ f_y(z, z_a) &= \frac{G}{\pi(1+\kappa)} \left(\frac{1}{z - z_a} + \frac{1}{\overline{z} - \overline{z_a}} + e^{2\mathrm{i}\theta} \left[\frac{1}{z - z_a} - \frac{(\overline{z} - \overline{z_a})}{(z - z_a)^2} \right] \right). \end{aligned} \tag{6}$$

2.1. Modeling of railheads containing surface and internal cracks

Figure 1 shows a railhead containing a surface crack and an internal crack. The railhead is loaded by the wheel on the top of the railhead. The problem is modelled by four cracks in an infinite plane. The first two cracks, C_1 and C_2, are curved cracks with the same shape as the profile of the railhead. The other two cracks, C_3 and C_4, are straight cracks modelling the surface and internal cracks. The loading is applied to the curved crack faces.

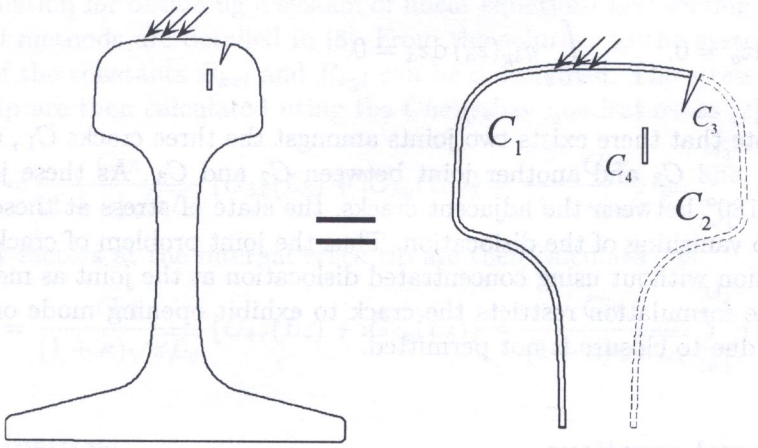

Fig. 1. Modeling of railhead under contact loading

For simplicity, the contact loading on the top of the railhead is simplified as a uniform pressure loading as shown in Fig. 1, although any distribution could easily be accommodated. The railhead stresses are of primary interest in this paper; the boundary condition along the rail base does not influence significantly the railhead stress field and hence has not been modelled exactly. To simplify the analysis, the boundary condition of the lower part of the rail-body was assumed as being connected to the infinite plane.

Furthermore, the four cracks are modelled by continuously distributed dislocation along the line at the location of the cracks. The distribution functions of Burgers vector β_x and β_y are denoted by $g_{kx}(z_a)$ and $g_{ky}(z_a)$ along C_k $(k = 1, 2, 3, 4)$. The normal and tangential stress components at a point z on C_j $(j = 1, 2, 3, 4)$ induced by the distributed dislocation are obtained from an integral of the stress induced by the dislocation at pointz_a as shown in Eq. (7),

$$\sigma_{nn(jk)}(z) + \mathrm{i}\tau_{nt(jk)}(z) = \int_{C_k} \left[g_{kx}(z_a)\, f_{kx}(z, z_a) + g_{ky}(z_a)\, f_{ky}(z, z_a) \right] \mathrm{d}z_a \,. \tag{7}$$

$f_{kx}(z, z_a)$ and $f_{ky}(z, z_a)$ are derived directly from Eq. (6).

Superposition of the stress at the j-th crack induced from distributed dislocation along the four cracks should meet the boundary conditions along the crack faces. This leads to integral equations as defined in Eq. (8),

$$\sum_{k=1}^{4} \int_{C_k} [g_{kx}(z_a)\, f_{kx}(z, z_a) + g_{ky}(z_a)\, f_{ky}(z, z_a)]\, dz_a = p_{nn(j)}(z) + \mathrm{i} p_{nt(j)}(z) \qquad (8)$$

$$z \text{ on } C_j\,, \quad j = 1, 2, 3, 4$$

where $p_{nn(j)}(z) + \mathrm{i} p_{nt(j)}(z)$ are external boundary tractions prescribed to faces of the j-th crack whose value are equal to the external normal and tangential tractions if z is on the loaded crack face segment, or equal to zero if z is on the traction free segments,

$$p_{nn(j)}(z) + \mathrm{i} p_{nt(j)}(z) = \begin{cases} p_{nn}(z) + \mathrm{i} p_{nt}(z) & z \text{ on loading segment,} \\ 0 & z \text{ on traction free segment.} \end{cases} \qquad (9)$$

The single-valued displacement conditions around the railhead surface and the internal crack also lead to a set of integral equations as

$$\begin{aligned} &\sum_{k=1}^{3} \int_{C_k} g_{kx}(z_a)\, \mathrm{d}z_a = 0, \qquad \int_{C_4} g_{4x}(z_a)\, \mathrm{d}z_a = 0, \\ &\sum_{k=1}^{3} \int_{C_k} g_{ky}(z_a)\, \mathrm{d}z_a = 0, \qquad \int_{C_4} g_{4y}(z_a)\, \mathrm{d}z_a = 0. \end{aligned} \qquad (10)$$

It is worth to note that there exists two joints amongst the three cracks C_1, C_2 and C_3, namely a joint between C_1 and C_3 and another joint between C_2 and C_3. As these joints always define an angle less than 180° between the adjacent cracks, the state of stress at these joints will remain zero, which leads to vanishing of the dislocation. Thus the joint problem of crack is simulated using distributed dislocation without using concentrated dislocation at the joint as modelled in [11]. This simplification in the formulation restricts the crack to exhibit opening mode only; in other words crack face traction due to closure is not permitted.

2.2. Singular integral equations

The set of integral equations shown in Eqs. (8) and (10) provide the basis for solving the original problem. The right side of these equations and the kernel functions ($f_{kx}(z, z_a)$ and $f_{ky}(z, z_a)$) in the left side of these equations are known functions, while the dislocation distribution functions, $g_{kx}(z_a)$ and $g_{ky}(z_a)$ are unknown functions to be determined.

From Eq. (6), it can be seen that Eq. (8) is a set of singular integral equations, because the kernel functions, $f_{kx}(z, z_a)$ and $f_{ky}(z, z_a)$, are singular when z tends to z_a. It has been reported that the kernel in Eq. (8) is the Cauchy type when the integral contour is a straight line [12], and Hilbert type when the contour is a circle [7]. For arbitrarily shaped integral contours, the kernel functions vary directly depending on the shapes of the cracks [8]. However, as the order of these kernel functions does not change, we can reduce them to products of the Cauchy kernel with normal functions.

The coordinates z_k of a point on the crack C_k are expressed by a function $z_k = z_k(\zeta_k)$ in term of a variable ζ_k which is the length from midpoint of C_k to the point z. When z moves to z_a, the magnitude of variable ζ_k will be equal to s_k. Using the introduced function and variable, the kernel functions are expanded into products of the Cauchy kernel with normal functions, $F_{kx}(\zeta_k, s_k)$ and $F_{ky}(\zeta_k, s_k)$. The normal functions are further expanded into two-dimensional first kind Chebyshev series. The parameters for the series are calculated from Eq. (6). The solutions of the dislocation

distribution functions, $g_{kx}(s)$ and $g_{ky}(s)$, at crack tips are dominated by the square root singularity, thus the functions are given in the form of

$$g_{kx}(s_k) = \frac{G_{kx}(s_k)}{\sqrt{L_k^2 - s_k^2}},$$
$$g_{ky}(s_k) = \frac{G_{ky}(s_k)}{\sqrt{L_k^2 - s_k^2}}, \tag{11}$$
$$-L_k \le s_k \le L_k, \quad k = 1, 2, 3, 4,$$

where $G_{kx}(s_k)$ and $G_{ky}(s_k)$ are two unknown normal functions to be solved, which are expanded into the first kind of the Chebyshev series as shown in Eq. (12)

$$G_{kx}(s_k) = \sum_{l=0}^{M} B_{kxl} T_l\left(\frac{s_k}{L_k}\right),$$
$$G_{ky}(s_k) = \sum_{l=0}^{M} B_{kyl} T_l\left(\frac{s_k}{L_k}\right), \tag{12}$$
$$k = 1, 2, 3, 4,$$

where $T_l(\frac{s_k}{L_k})$ is the l-th order Chebyshev polynomial and B_{kxl} and B_{kyl} are constants to be determined.

Complete formulation for obtaining a system of linear equations and solving the equations using standard numerical methods are detailed in [8]. From the solution to the system of equations, the numerical results of the constants B_{kxl} and B_{kyl} can be determined. The stress intensity factors at the surface crack tip are then calculated using the Chebyshev quadrature as [2]

$$K = K_I - \mathrm{i}K_{II} = \frac{G\mathrm{i}\pi}{(1+\kappa)\sqrt{\pi L_3}} \{G_{3x}(L_3) + \mathrm{i}G_{3y}(L_3)\} = \frac{G\mathrm{i}\pi}{(1+\kappa)\sqrt{\pi L_3}} \sum_{l=1}^{M_3} (B_{3xl} + \mathrm{i}A_{3yl}). \tag{13}$$

The stress intensity factors at the internal crack tip are then calculated as

$$K = K_I - \mathrm{i}K_{II} = \frac{G\mathrm{i}\pi}{(1+\kappa)\sqrt{\pi L_4}} \{G_{4x}(L_4) + \mathrm{i}G_{4y}(L_4)\} = \frac{G\mathrm{i}\pi}{(1+\kappa)\sqrt{\pi L_4}} \sum_{l=1}^{M_4} (B_{4xl} + \mathrm{i}A_{4yl}). \tag{14}$$

3. Numerical results

A standard AS60 kg/m railhead subjected to wheel loading at the gauge corner as shown in Fig. 2 was considered for the numerical examples presented in this section. The loading is simplified as the uniformly distributed pressure along the normal and tangential directions of the railhead profile. The ratio between normal and tangential pressure is assumed to remain constant (0.3) in all cases analysed. The Poisson's ratio is 0.3 and the strain state is assumed plane strain.

Six examples, each considering a specific case of crack is presented. The first example identifies the worst possible orientation of the surface crack located just under the loading in the gauge corner. The second example examines the worst possible orientation of the internal crack when the surface crack orientation remains fixed at the value determined in example one. For this purpose, the lengths of the surface and internal cracks and the distance between the centers of the two cracks were kept constant. The third example examines the effect of the distance between the tips of the surface and the internal cracks when the two respective cracks remain at a constant orientation identified in example two.

The last three examples consider the cracks along the symmetric vertical axis whilst the loading remains at the gauge corner. Example four examines the sensitivity of the angle of inclination of the internal crack with respect to the surface crack. Example five considers sensitivity of distance between the two cracks and example six investigates the sensitivity of the internal crack length.

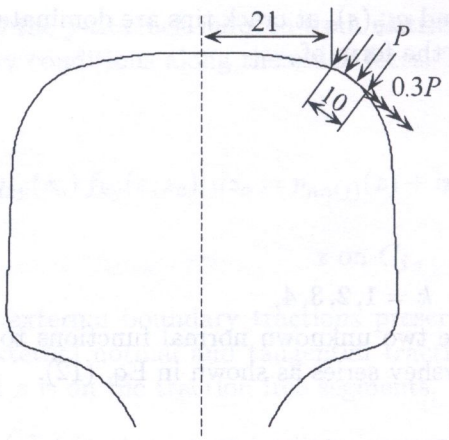

Fig. 2. AS60 kg/m railhead and loading at gauge corner

3.1. Example #1

The first example deals with a surface crack at the gauge corner. No internal crack was considered in this example. To determine the angle at which the SIF of the surface crack had a maximum value, the angle of inclination of the surface crack, θ (measured from the tangential axis as shown in Fig. 3) was varied from the minimum possible angle (50°) to the maximum possible angle (138°) permitted by the profile of the rail gauge corner. The calculated stress intensity factors were normalised by $K^0 = P\sqrt{2\pi a_3}$.

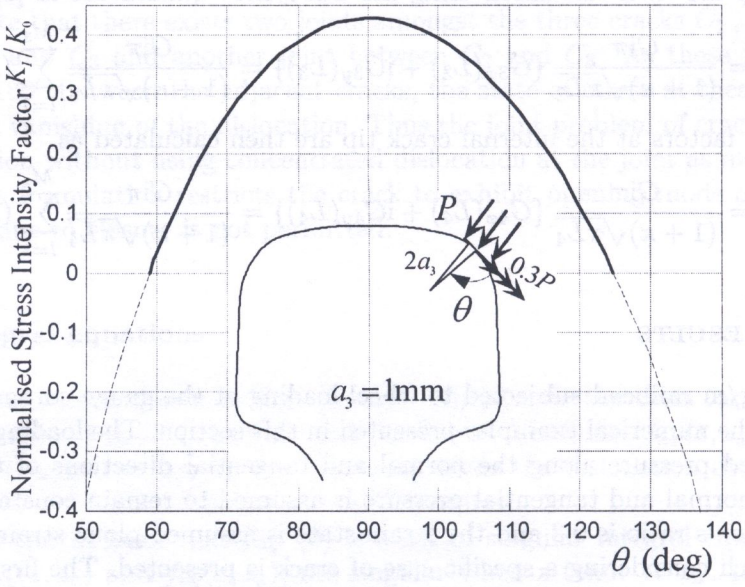

Fig. 3. Model I SIF of surface crack tip varies against the incline angle

Figure 3 shows that the normalised Mode I SIF varies against the angle θ. With the increase in the angle the Mode I SIF has increased, and reached a maximum value when $\theta = 90°$. This shows that the normal direction to the gauge corner (or parallel to the direction of the loading) is the easiest direction for the propagation of surface crack. For the range of angles from 59° to 124°, the SIF shown by thick solid line in Fig. 3 remains positive. However, for all other angles, the SIF was negative, as shown by the dashed lines in Fig. 3 (which shows inappropriate solutions for the theory presented in this paper due to the fact that the crack faces near the tips for these cases are no longer traction-free).

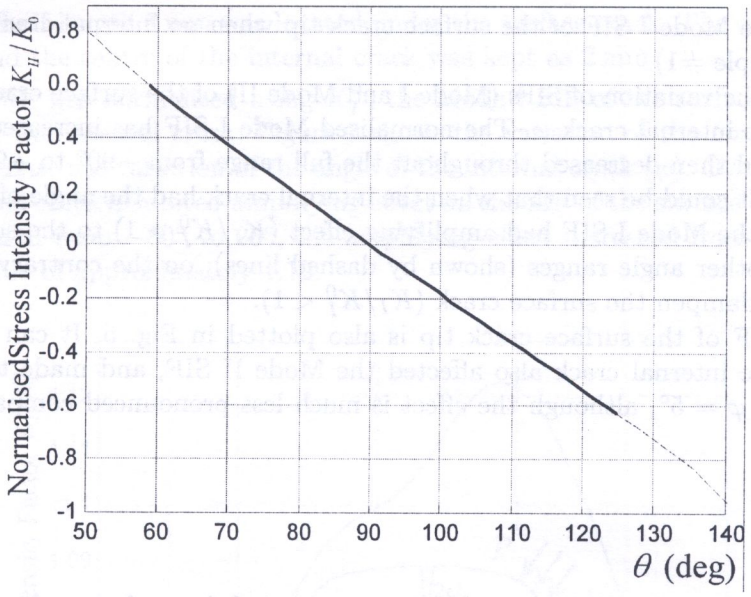

Fig. 4. Model II SIF of the surface crack tip varies against the incline angle θ

Figure 4 shows the variation of Mode II SIF against the angle of inclination of the surface crack. The Mode II SIF has decreased over the full range of the angle as shown in Fig. 4. When $\theta = 90°$, the Mode II SIF is zero has vanished, confirming Mode I crack growth as shown in Fig. 3.

3.2. Example #2

The second numerical example considers an internal crack with half-length 1 mm interacting with a surface crack whose angle of inclination θ was fixed at 90°. The internal crack was located under the surface crack at a distance of 2 mm between the surface crack tip and the center of the internal crack. The internal crack was allowed to rotate from −90° to +90°. The calculated SIF is normalised

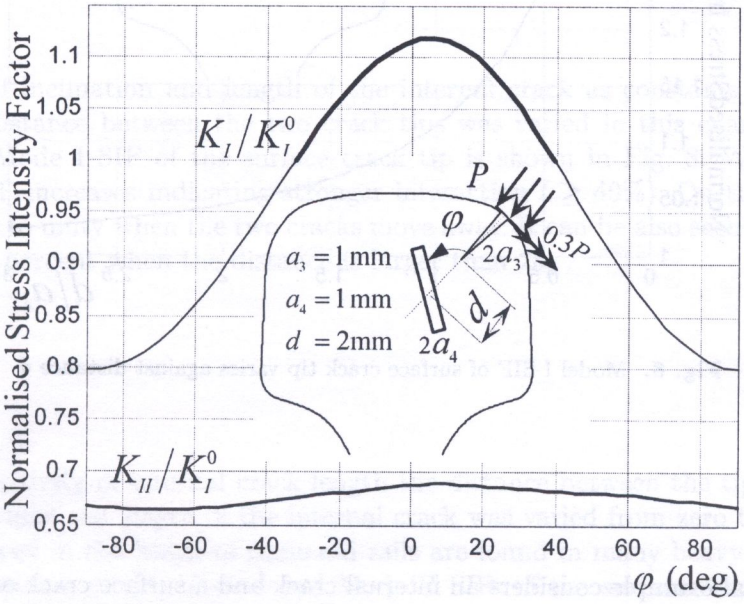

Fig. 5. SIFs of surface crack tip varies against incline angle of internal crack

by K_I^0, which is the Mode I SIF of the surface crack tip when no internal crack was considered in the railhead (Example #1).

Figure 5 shows the variation of SIFs (Mode I and Mode II) of the surface crack against the angle of inclination of the internal crack φ. The normalised Mode I SIF has increased when φ increased from $-90°$ to $5°$ and then decreased throughout the full range from $-90°$ to $+90°$, the Mode I SIF remained positive. It could be seen that when the internal crack had the angle of inclination ranging from $-32°$ to $39°$, the Mode I SIF had amplifying effect ($K_I/K_I^0 > 1$) to the surface crack. For all other case, in the other angle ranges (shown by dashed lines), on the contrary, the internal crack had a tendency to dampen the surface crack ($K_I/K_I^0 < 1$).

The Mode II SIF of the surface crack tip is also plotted in Fig. 5. It can be seen that angle of inclination of the internal crack also affected the Mode II SIF, and made the SIF reaching its maximum value at $\varphi = 5°$, although the effect is much less pronounced compared to the effect of the Mode I SIF.

3.3. Example #3

Figure 6 shows the sensitivity of the distance between tips of the surface and internal cracks on the Mode I SIF of the surface crack tip when the surface crack angle θ was $90°$ and the internal crack angle φ was zero degree. The half lengths of the two cracks were kept as 1 mm. As shown in Fig. 6, the normalised Mode I SIF has decreased sharply when the distance increased from zero. When the distance is larger than $2a_4$, the interaction was less than 5 percent (insignificant). The proximity of the internal crack is hence clearly shown to be important for any acceleration of the growth of the surface crack.

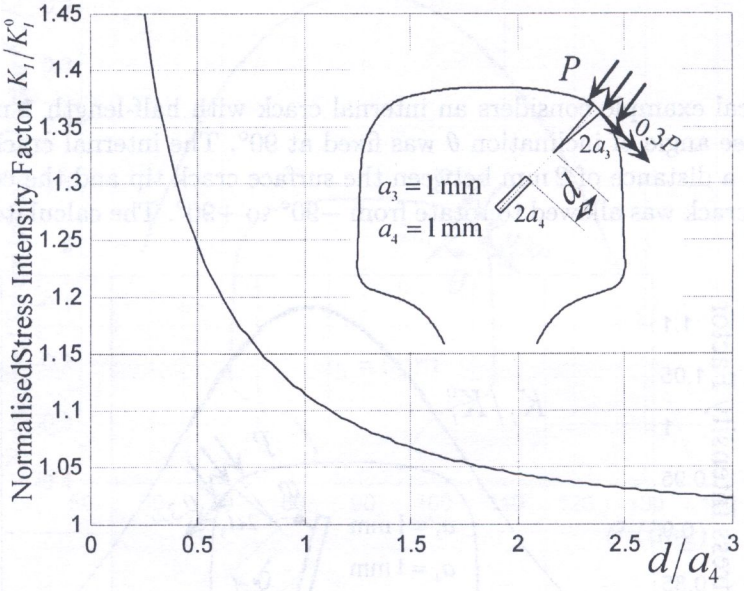

Fig. 6. Model I SIF of surface crack tip varies against distance d

3.4. Example #4

The fourth numerical example considers an internal crack and a surface crack on the vertical centre line of the railhead whilst the loading remained at the gauge corner as in the previous examples. Length and the angle of inclination of the surface crack was kept as 2 mm and $90°$ respectively. The

internal crack with half-length 1 mm was located under the surface crack. The distance between the surface crack tip and the centre of the internal crack was kept as 2 mm.

The calculated SIF was normalised using K_I^0, the Mode I SIF of the surface crack without the interaction effect of the internal crack. Figure 7 shows the variation of the normalised SIF for the surface crack tip against the variation of the angle of the internal crack (φ). Over the entire range of the angle, the internal crack exhibited amplifying effect on the SIF of the surface crack ($K_I/K_I^0 > 1$). As the angle increased from $-80°$ to $25°$, the amplifying effect increased from its minimum value to its maximum value of approximately 1.12.

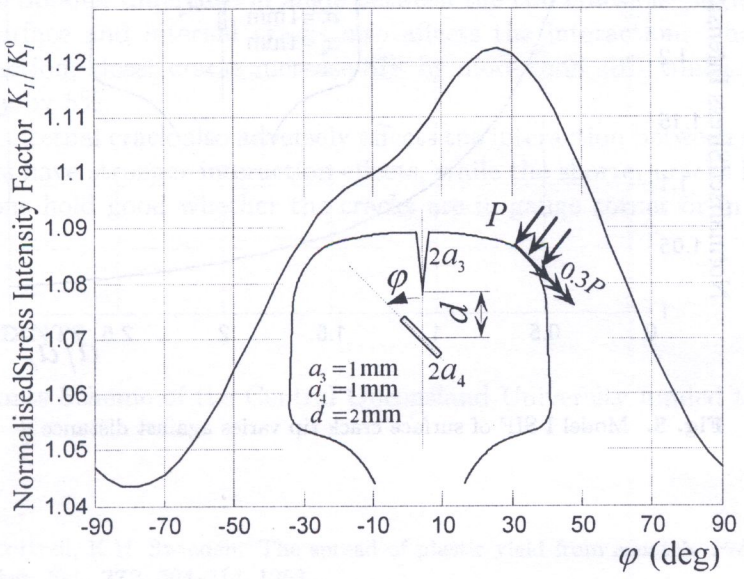

Fig. 7. SIFs of surface crack tip varies against incline angle of internal crack

3.5. Example #5

Setting the angle of inclination and length of the internal crack as constants ($\varphi = 0°$ and 2 mm respectively), the distance between the two crack tips was varied in this example. The variation of the normalised Mode I SIF of the surface crack tip is shown in Fig. 8. When the two cracks move closer, the SIF increases indicating stronger interaction ($\geq 40\%$). On the contrary, the SIF decreases and tends to unity when the two cracks move away. It can be also seen that the interaction effect is less than 5 percent when the distance is larger than $2a_4$.

3.6. Example #6

To consider the sensitivity of internal crack length the distance between the tips of the two cracks are fixed as 1 mm whilst the length of the internal crack was varied from zero to 20 mm (such long cracks centrally placed in the heads of some old rails are found in many heavy haul tracks around the world). The variation of the Mode I and Mode II SIFs of the surface crack is calculated and plotted in Fig. 9. As the length increases, both Mode I and Mode II SIFs increase. Thus the larger the internal crack, the stronger the interaction with the surface crack.

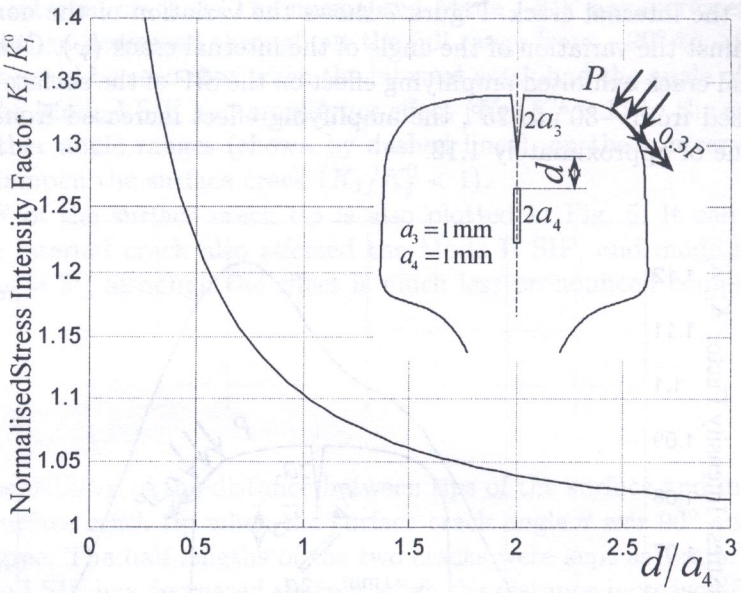

Fig. 8. Model I SIF of surface crack tip varies against distance d

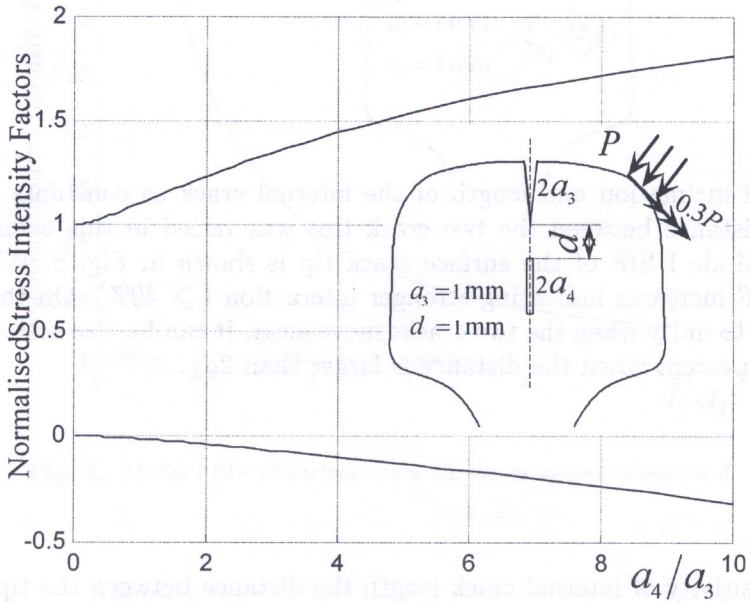

Fig. 9. Model I SIF of surface crack tip varies against internal crack length

4. Conclusions

A continuous distributed dislocation method formulated for arbitrary shaped 2D crack problems by the authors recently has been extended with particular reference to modeling the interaction problem between surface and internal cracks in railhead. This method can also treat interaction among curved cracks with arbitrary shape in a finite body.

From the numerical results, we found that the internal subsurface cracks interact with surface cracks in a way that is of practical relevance. The interaction depends on the location and geometry of the internal cracks. Angle of inclination of the internal crack has the potential to amplify the SIF of the surface crack tip. Smaller difference in angle between the two cracks is particularly detrimental. Distance between surface and internal cracks also affects the interaction. The closer the cracks, the higher the interaction; closer cracks increase SIF by more than 40% whilst the far-away cracks increase the SIF only by 5%.

The length of the internal crack also adversely affects the interaction between surface and internal cracks. Longer cracks have stronger interaction effects, while the shorter cracks have weaker effects. The above conclusions hold good whether the cracks are in gauge corner or in symmetric vertical axis of the railhead.

Acknowledgements

The RAAS 2003 Grants Scheme of the Central Queensland University funded this project.

References

[1] B.A. Bilby, A.H. Cottrell, K.H. Swinden. The spread of plastic yield from a notch. *Proc. Royal Soc. London, Series A: Math. Phys. Sci.*, **272**: 304–314, 1963.

[2] B.A. Bilby, J.D. Eshelby. Dislocations and the theory of fracture. In: H. Liebowitz, ed., *Fracture*, Vol. I, pp. 99–182. Academic Press, NY, 1968.

[3] Chen, Y.H., J.J. Han. Macrocrack-microcrack interaction in piezoelectric materials, Part I: Basic formulations and J-analysis. *ASME J. Appl. Mech.*, **66**: 514–521, 1999.

[4] Y.H. Chen, J.J. Han. Macrocrack-microcrack interaction in piezoelectric materials, Part II: Numerical results and discussions. *ASME J. Appl. Mech.*, **66**: 522–527, 1999.

[5] F. Erdogan, G.D. Gupta, M. Ratwani. Interaction between a circular inclusion and an arbitrarily oriented crack. *ASME J. Appl. Mech.*, **41**: 1007–1013, 1974.

[6] S.X. Gong, H. Horii. General solution to the problem of microcracks near the tip of a main crack. *J. Mech. Phys. Struct.*, **37**: 27–46, 1989.

[7] J.J. Han, Y.H. Chen. Interface crack interacting with a microvoid in the near-tip process zone. *Int. J. Fract.*, **102**: 223–244, 2000.

[8] J.J. Han, M. Dhanasekar. Modelling cracks in arbitrarily shaped finite bodies by distribution of dislocation. *Int. J. Solids Struct.*, **41**: 399–411, 2004.

[9] H. Horii, S. Nemat-Nasser. Elastic fields of interacting inhomogeneities. *Int. J. Solids Struct.*, **21**: 731–745, 1985.

[10] M. Horii, S. Nemat-Nasser. Interacting micro-crack near the tips in the process zone of a macro-crack. *J. Mech. Phys. Struct.*, **35**: 601–629, 1987.

[11] Q.H. Qin, X. Zhang. Crack deflection at an interface between dissimilar piezoelectric materials. *Int. J. Fract.*, **102**: 355–370, 2000.

[12] L.G. Zhao, Y.H. Chen. On the contribution of sub interface microcracks near the tip of a macrocrack to the J-integral in the bi-material solids. *Int. J. Engrg. Sci.*, **35**: 387–407, 1997.